Study of the Ferroelectric Liquid Crystal 11EB1M7 by Means of ^{2}H NMR†

Donata Catalano,‡ Leonardo Chiezzi,§ Valentina Domenici,§ Marco Geppi,§ and Carlo Alberto Veracini*

Dipartimento di Chimica e Chimica Industriale, Università degli Studi di Pisa, via Risorgimento 35, 56126 Pisa, Italy

Received: February 5, 2003; In Final Form: July 1, 2003

In this work, a new procedure for the synthesis of the selectively deuterium-labeled chiral liquid crystal (+)-(*S*)-4-[4′-(1-methylheptyloxy)] biphenyl 4-(10-undecenyloxy)benzoate (11EB1M7) has been developed, aimed to the study of its structure, orientational ordering, and dynamic behavior by means of ^{2}H NMR. 11EB1M7 was investigated throughout its mesophasic range, formed by a very rich variety of chiral liquid crystalline phases including blue, cholesteric, TGBA*, and smectic C*. Two isotopomers were synthesized by labeling 11EB1M7 on either the phenyl or the biphenyl moiety of the mesogenic core. This allowed structural information (such as the tilt angle of the rigid fragments of the molecule and the angle between their para axes), orientational order parameters, and individual diffusional coefficients for the various overall and internal motions to be obtained from ^{2}H NMR spectra and relaxation measurements by applying suitable data analyses based on several theoretical models.

Introduction

Chiral smectogens originating ferroelectric (FLC) and antiferroelectric (AFLC) phases represent a very interesting class of compounds because of their possible technological applications. In this context, the rationalization of the links between their macroscopic behavior and their compositional, structural, and dynamic properties at a molecular level is fundamental.[1]

NMR has been largely applied to the investigation of structure, orientational ordering,[2] and dynamics[3,4] of low-molecular-weight achiral liquid crystals and, more recently, has been revealed to be very effective for similar studies on chiral liquid crystals.[5] ^{2}H techniques are particularly powerful because of the intramolecular nature of the dominant quadrupolar interaction bringing about a quite straightforward interpretation of both static spectra and relaxation measurements and allowing structural and dynamic site-specific information to be obtained. However, the use of deuterium NMR is strongly limited by the requirement of purposely and selectively ^{2}H-labeled molecules.

Following previous works[6−10] based on the synthesis of selectively deuterium-labeled FLCs and the investigation of their structural, ordering, and dynamic properties, we report here an extension of such studies to 4-[4′-(1-methyl heptyloxy)] biphenyl 4-(10-undecenyloxy) benzoate (11EB1M7), for which two optically pure isotopomers, partially deuterated in either the phenyl or the biphenyl moieties (11EB1M7-d_2 and 11EB1M7-d_8, respectively), were prepared (see Figure 1). This FLC is particularly interesting because it exhibits a very rich variety of mesophases: blue phase, N*, TGBA*, SmA, SmC*, and SmI*. Moreover in this mesogen, contrary to those previously investigated, the achiral alkylic chain ends with a double bond, therefore allowing its use for the synthesis of corresponding side-chain liquid crystalline polymers, based on polysiloxane main chains, which have been shown to retain ferroelectric properties.[11]

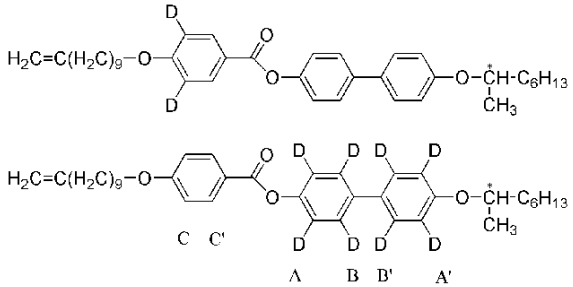

Figure 1. Molecular structure of the isotopomers 11EB1M7-d_2 (top) and 11EB1M7-d_8 (bottom).

In the first part of the paper, a ^{2}H NMR investigation of phase transitions, structural properties (tilt angle in the chiral smectic C* phase and angle between the para axes of the phenyl and biphenyl moieties in the untilted smectic phases), and ordering behavior (order parameter S_{ZZ} and biaxiality of the phenyl and biphenyl moieties) of 11EB1M7 are reported. In the second part, the molecular dynamics of 11EB1M7 was studied by means of ^{2}H NMR relaxation measurements. In the SmA phase, diffusional coefficients for individual internal (rotations of the aromatic fragments around their para axes) and overall (spinning and tumbling) molecular motions could be determined applying suitable theoretical models.

Experimental Section

Synthesis. The schemes of the reactions carried out to synthesize 11EB1M7-d_2 and 11EB1M7-d_8 are reported in Figures 2 and 3, respectively.

(−)(R)-2-Octyl-p-toluensulfonate (2). (−)(*R*)-2-octanol (**1**) (7 mL, 44.2 mmol) and *p*-toluensulfonyl chloride (8.8 g, 46.3

† Dedicated to the memory of Prof. S. Castellano.

* To whom correspondence should be addressed. Phone number: +39-050918266. Fax number: +39-050918260. E-mail address: verax@dcci.unipi.it.

‡ Phone number: +39-050918266. E-mail address: donata@dcci.unipi.it.

§ Phone number: +39-050918289. E-mail addresses: leonardo@dcci.unipi.it (L.C.); valentin@dcci.unipi.it (V.D.); mg@dcci.unipi.it (M.G.).

10.1021/jp034301h CCC: $25.00
Published on Web 08/23/2003

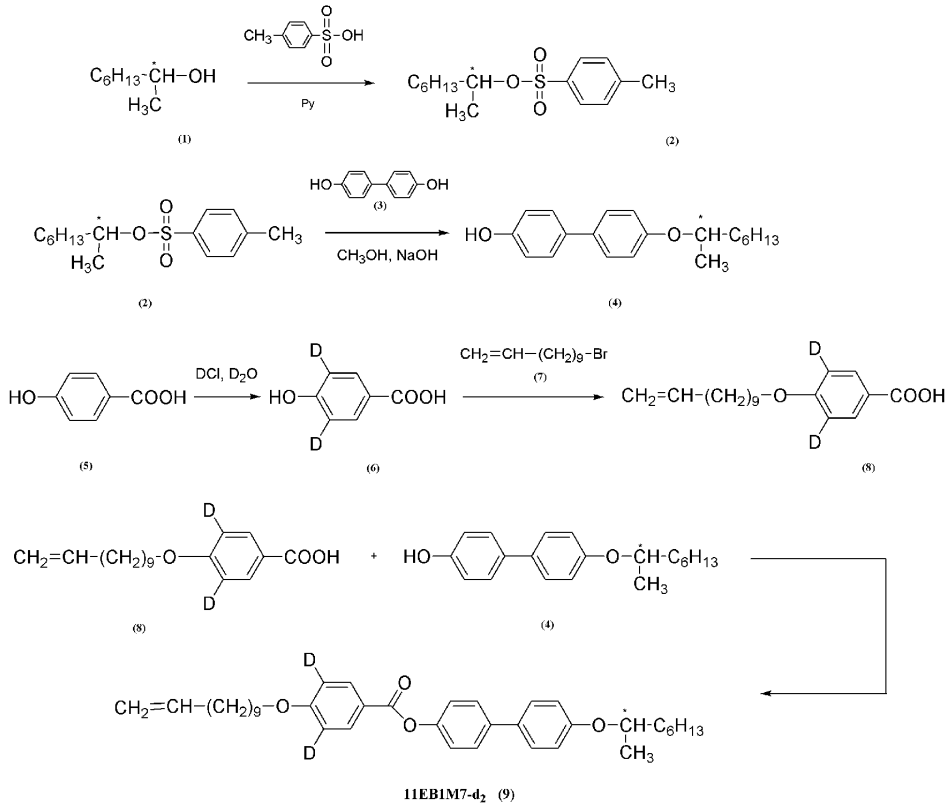

Figure 2. Reaction scheme for the synthesis of 11EB1M7-d_2.

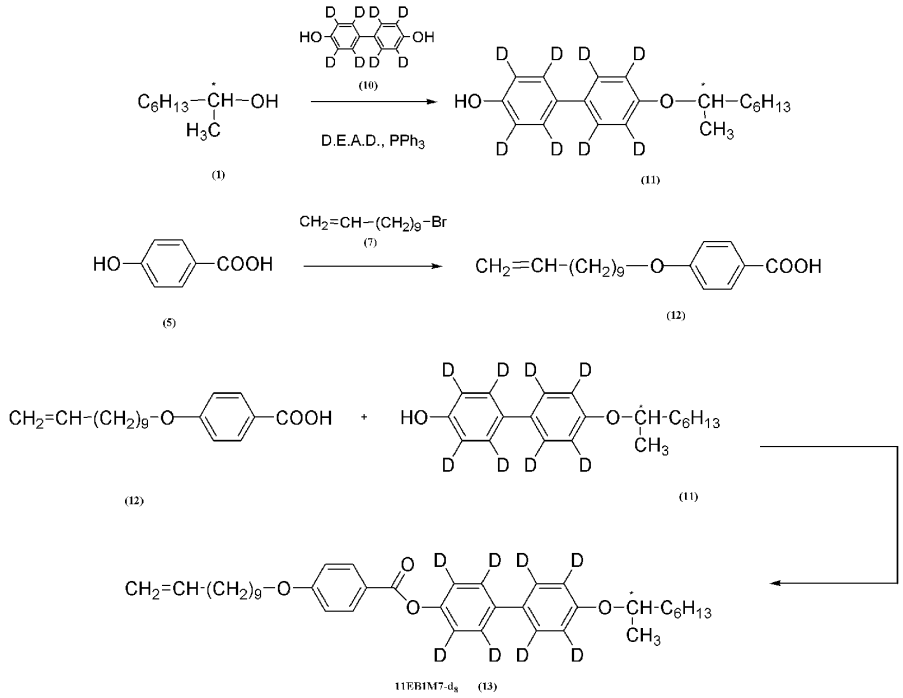

Figure 3. Reaction scheme for the synthesis of 11EB1M7-d_8.

mmol) were dissolved in 27 mL of anhydrous pyridine under nitrogen atmosphere at 0 °C. The solution was stirred at room temperature for 18 h, and then 120 mL of water was added, and the aqueous phase was extracted with chloroform. The organic layers were washed with a solution of HCl 3 N and dried over magnesium sulfate and then evaporated. A yellow oil was obtained (8.9 g, yield 71%). ^{1}H NMR ($CDCl_3$): δ = 7.78 (2H, d), 7.32 (2H, d), 4.55 (1H, m), 2.45 (3H, s),1.7−1.0 (13H, m), 0.92 (3H, t).

*(+)(S)-4-hydroxy-4′-(1-methyleptyl)biphenol (**4**).* 4,4′-Dihydroxybiphenol (**3**) (5.7 g, 30.8 mmol) and sodium hydroxide (1.3 g, 33.1 mmol) were dissolved in 70 mL of methanol. The solution was refluxed for 30 min, and then a solution of 8.7 g (30.7 mmol) of (−)(*R*)-2-octyl-*p*-toluensulfonate (**2**) in 20 mL of methanol was added drop by drop. The solution was refluxed for 12 h, and then 110 mL of water was added, and the organic phases were extracted with chloroform, dried over magnesium sulfate, and evaporated. The resulting solid material was purified

by chromatography on a Kieselgel 60 (0.063−0.02 mm) column and eluted with petroleum ether and ethyl acetate (4:1) to give 2.6 g of a white solid (yield 28%). $[\alpha]^{20}_{589}$ (deg·dm^{-1}·g^{-1}·cm^3) = 5 (c = 1% $CHCl_3$). ^{1}H NMR ($CDCl_3$): δ = 7.43 (4H, m), 6.90 (4H, m), 4.32 (1H, m), 2.0−1.1 (13H, m), 0.88 (3H, t).

*4-Hydroxy Benzoic Acid-d_2 (**6**).* 4-Hydroxy benzoic acid (**5**) (4.0 g, 29.1 mmol) was dissolved in 50 g of a solution at 8% of deuterium chloride. The solution was refluxed for 24 h, and then the mixture was cooled at 0 °C, and the white solid formed was filtered and dried. A total of 3.4 g (yield 84%) of **6** was obtained. ^{1}H NMR (DMSO-d_6): δ = 12.4 (1H, broad s), 10.2 (1H, broad s), 7.77 (2H, s + very weak d), 6.80 (0.1H, d). From the ^{1}H NMR spectrum, 95% deuteration was estimated.

*4-n-Undecenyloxy Benzoic Acid-d_2 (**8**).* 4-Hydroxy benzoic acid-d_2 (**6**, 3.4 g, 24 mmol) and potassium hydroxide (3.7 g, 66 mmol) were dissolved in 40 mL of a mixture of water and ethanol, 9:1. The solution was refluxed for 20 min; then 7.0 mL (33.3 mmol) of undecenyl bromide (**7**) was added drop by drop. The solution was refluxed for an additional 4 h; then HCl 1 N was added until pH = 5. The white solid that precipitated was filtered and washed with water. The solid was further purified by recrystallization from ethanol. A total of 3.9 g (yield 56%) of **8** was obtained. ^{1}H NMR (DMSO-d_6): δ = 12.4 (1H, broad s), 7.85 (2H, s + very weak d), 6.97 (0.1H, d), 5.76 (1H, m), 4.95 (2H, m), 4.00 (2H, t), 2.1−1.0 (16H, m).

*(+)(S)-4-[4′-(1-Methyl Heptyloxy)] Biphenyl 4-(10-Undecenyloxy)benzoate-d_2 (**9**).* (+)(*S*)-4-Hydroxy-4′-(1-methyleptyl)-biphenol (**4**, 2.0 g, 6.7 mmol), 4-*n*-undecenyloxy benzoic acid-d_2 (**8**, 2.0 g, 6.7 mmol), and a catalytic amount of 4-dimethylamino pyridine (DMAP) were dissolved in 90 mL of anhydrous dichloromethane under nitrogen atmosphere. A solution of 1.4 g (6.7 mmol) of dicyclohexyl carbodimmyde (DCC) in 20 mL of anhydrous dichloromethane was added drop by drop to the mixture. The solution obtained was stirred at room temperature for 3 days; then the precipitate was filtered off, and the organic phases were washed with HCl 1 N and with a 5% solution of $NaHCO_3$, dried over magnesium sulfate, and evaporated. A total of 3.28 g (yield 86%) of **9** was obtained after two recrystallizations in ethanol. $[\alpha]^{20}_{589}$ (deg·dm^{-1}·g^{-1}·cm^3) = 4.8 (c = 1% $CHCl_3$). ^{1}H NMR ($CDCl_3$): δ = 8.18 (2H, s + very weak d), 7.57 (4H, m), 7.24 (2H, d), 6.98 (2H, d), 5.81 (1H, m), 4.95 (2H, m), 4.40 (1H, m), 4.04 (2H, t), 2.2−1.0 (29H, m), 0.90 (3H, t).

*4,4′-Dihydroxybiphenol-d_8 (**10**).* Sodium (4.9 g, 213 mmol) was dissolved in small portions in 200 mL of ethanol under cooling, and then 4,4′-dihydroxybiphenol (20.0 g, 107.4 mmol) was added under nitrogen atmosphere. This solution was evaporated, and the solid material obtained was dissolved in 100 mL of D_2O (5 mol) and put in an autoclave with 1 g of Pt/C. The autoclave was heated to 200 °C (7 bar) for 3 days. The cooled reaction mixture was evaporated and treated with diethyl ether, and the catalyst was filtered off. The organic layers were washed with HCl 1 N, dried over magnesium sulfate, and evaporated. A total of 9.1 g (yield 45%) of 4,4′-dihydroxybiphenol-d_8 (**10**) was obtained. ^{1}H NMR (DMSO-d_6): δ = 9.15 (2H, s), 7.33 (3.28H, m), 6.81 (0.72H, m). From ^{1}H NMR, the following percentages of deuteration were obtained: 82% for the ortho positions marked A and A′ in Figure 1 and 18% for the meta positions B and B′.

*(−)(R)-4-Hydroxy-4′-(1-methyleptyl)biphenol-d_8 (**11**).* 4,4′-Dihydroxybiphenol-d_8 (**10**, 4.5 g, 23.2 mmol), triphenyl phosphine (6 g, 23.2 mmol), and diethyl azodicarboxylate (D.E.A.D., 4 g, 23.2 mmol) were dissolved in 80 mL of anhydrous THF under nitrogen atmosphere. A solution of (−)(*R*)-2-octanol (**1**) (3 g, 23.2 mmol) in 20 mL of anhydrous THF was added drop by drop to the mixture. The solution obtained was stirred at room temperature for 5 days; then the THF was evaporated, diethyl ether was added, and the white precipitate obtained was filtered off. The organic phases were evaporated, and the product was purified by chromatography on Kieselgel 60 (0.063−0.02 mm) column and eluted with petroleum ether and ethyl acetate (4:1) to give 3.4 g of a white solid (yield 56%). $[\alpha]^{20}_{589}$ (deg·dm^{-1}·g^{-1}·cm^3) = −5 (c = 1% $CHCl_3$). ^{1}H NMR ($CDCl_3$): δ = 7.44 (3.28H, m), 6.90 (0.72H, m), 4.37 (1H, m), 2.0−1.1 (13H, m), 0.88 (3H, t).

*4-n-Undecenyloxy Benzoic Acid (**12**).* 4-Hydroxy benzoic acid (**5**, 2.0 g, 15 mmol) and potassium hydroxide (2 g, 36 mmol) were dissolved in 40 mL of a mixture of water and ethanol, 9:1. The solution was refluxed for 20 min; then 4 mL (19 mmol) of undecenyl bromide (**7**) was added drop by drop. The solution was refluxed for additional 4 h; then HCl 1 N was added until pH = 5. The white solid precipitate obtained was filtered and washed with water. The solid was further purificated by recrystallization from ethanol; 2.5 g (yield 58%) of (**12**) were obtained. ^{1}H NMR (DMSO-d_6): δ = 12.4 (1H, broad s), 7.85 (2H, d), 6.97 (2H, d), 5.76 (1H, m), 4.95 (2H, m), 4.00 (2H, t), 2.1−1.0 (16H, m).

*(−)(R)-4-[4′-(1-Methyl Heptyloxy)] Biphenyl 4-(10-Undecenyloxy)benzoate-d_8 (**13**).* (−)(*R*)-4-Hydroxy-4′-(1-methyleptyl)-biphenol-d_8 (**11**, 2 g, 6.5 mmol), 4-*n*-undecenyloxy benzoic acid (**12**, 1.9 g, 6.5 mmol), and a catalytic amount of 4-dimethylamino pyridine (DMAP) were dissolved in 45 mL of anhydrous dichloromethane under nitrogen atmosphere. A solution of 1.4 g (6.5 mmol) of dicyclohexyl carbodimmyde (DCC) in 15 mL of anhydrous dichloromethane was added drop by drop to the mixture. The solution obtained was stirred at room temperature for 3 days; then the precipitated was filtered off, and the organic phases were washed with HCl 1 N and with a 5% solution of $NaHCO_3$, dried over magnesium sulfate, and evaporated. A total of 1.5 g (yield 40%) of **13** was obtained after two recrystallizations in ethanol. $[\alpha]^{20}_{589}$ (deg·dm^{-1}·g^{-1}·cm^3) = −4.8 (c = 1% $CHCl_3$). ^{1}H NMR ($CDCl_3$): δ = 8.18 (2H, d), 7.57 (3.28H, m), 7.24 (0.36H, m), 6.98 (2.36H, m), 5.81 (1H, m), 4.95 (2H, m), 4.40 (1H, m), 4.04 (2H, t), 2.2−1.0 (29H, m), 0.90 (3H, t) (The attribution of the aromatic signals is the following: 8.18 ppm (phenyl protons in position C′), 7.57 ppm (residual protons in positions B and B′), 7.24 ppm (residual protons in position A), and 6.98 ppm (residual protons in position A′ and phenyl protons in position C)).

Instrumentation. The calorimetric measurements were carried out on a Mettler TA4000 calorimeter. Optical textures were obtained by a Reichert-Jung Polyvar polarizing microscope equipped with a Mettler FP52 hot stage and Mettler FP5 temperature controller. ^{1}H NMR spectra were performed on a Varian VXR 300 spectrometer operating at 299.96 MHz on proton.

Phase Transitions. The following phase behavior has been found for the isotropomers 11EB1M7-d_2 and 11EB1M7-d_8, respectively, by optical microscopy and differential scanning calorimetry: I 115.9 °C, BPI 113.2 °C, N* 108.0 °C, TGBA* 102.0 °C, SmA 91.0 °C, SmC* 76.9 °C, SmI* 72.2°C Cr; I 111.4 °C, BPI 109.8 °C, N* 107.4 °C, TGBA* 103.1 °C, SmA 90.3 °C, SmC* 68.7 °C, SmI* 63.5 °C Cr. The following phase transitions were previously reported for the nondeuterated analogue:[12] I 115.2 °C, BPI 114.8 °C, N* 112.8 °C, TGBA* 107.0 °C, SmA 100.0 °C, SmC* 78.0 °C, SmI* 73.8 °C Cr.

^{2}H NMR. The ^{2}H NMR experiments were carried out on a 7.05 T Varian VXR-300 spectrometer working at 46.04 MHz

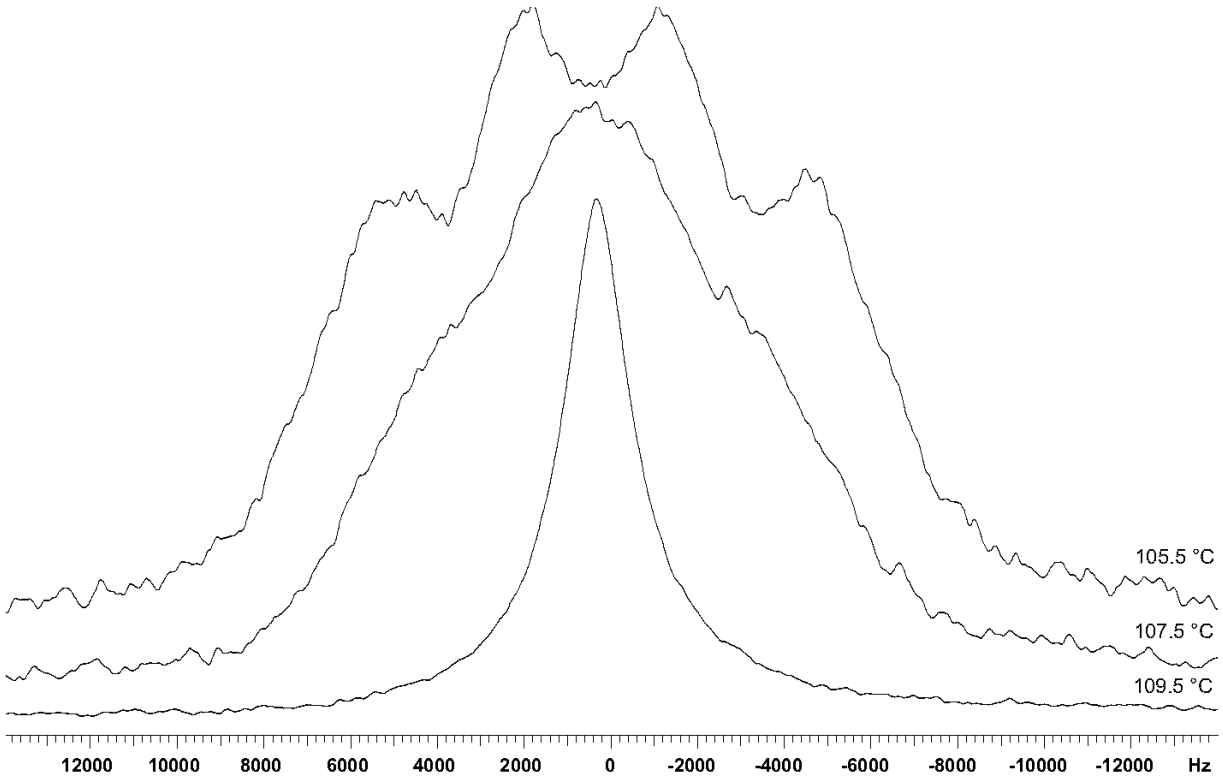

Figure 4. ^{2}H spectra of 11EB1M7-d_2 recorded, from bottom to top, in the blue phase at 109.5 °C, in the N* phase at 107.5 °C, and in the TGBA* phase at 105.5 °C.

for deuterium. The 90° pulse was 16 μs. The ^{2}H spectra were recorded either with or without ^{1}H continuous-wave decoupling. The samples were microscopically aligned within the magnet by slow cooling from the isotropic phase; the spectra were recorded every 2 °C allowing 10 min for thermal equilibration. The temperature was stable within 0.2 °C. In the interval between the isotropic and the smectic A phase, where blue, TGBA*, and N* phases could be observed, the spectra were recorded every 0.5 °C by both heating and cooling the sample: a difference in transition temperatures up to 2 °C was observed in the two cases.

^{2}H Zeeman (T_{1Z}) and quadrupolar (T_{1Q}) spin−lattice relaxation times were measured at 46.04 MHz at different temperatures within the mesophasic range through a broadband version[13] of the Jeener−Broekaert[14] pulse sequence (90_0-$2\tau_1$-67.5_{270}-$2\tau_1$-45_{90}-τ_1-45_{90}-τ_2-45_0) under proton decoupling. The best value of the delay τ_1 was experimentally found to be 13 μs. The variable delay τ_2 ranged from 100 μs to 1 s; a relaxation delay of 1 s and a number of scans of 1000 were used.

T_{1Z} and T_{1Q} were obtained by fitting the sum and difference of the integrals of each component of a quadrupolar doublet as a function of τ_2 through the following equations:[15]

$$M_+(\tau_2) = A[1 - B\exp(-\tau_2/T_{1Z})] \quad (1)$$

$$M_-(\tau_2) = C + D\exp(-\tau_2/T_{1Q}) \quad (2)$$

which differ from those theoretically predicted[16] because they take into account possible experimental imperfections.

Line Shape for the Blue, Cholesteric, and TGBA* Phases

The line shapes for the blue, cholesteric, and TGBA* phases are quite peculiar and even diagnostic of the type of mesophase itself, as evident from several studies present in the literature.[17−22] For the compound under study, a qualitative line shape analysis has been carried out, as previously done in a recent work for a similar chiral compound forming blue and cholesteric mesophases.[7] There are no significant differences between the line shapes of the two smectogens 11EB1M7-d_2 and 11EB1M7-d_8, except for a greater complexity in the case of the latter due to the superimposition of slightly different signals from the various deuteria; therefore, we only report the analysis of the ^{1}H-decoupled spectra of 11EB1M7-d_2.

The line shape of the blue phase is similar to that of the isotropic phase, but the line width is remarkably higher in the first case, around 1500 Hz instead of tens of hertz (see Figure 4). This can be explained by considering the nature of the blue phase, presumably an isotropic distribution of nematic domains.[17,18]

To explain the line shape typical of the cholesteric phase, the helicoidal path described by the local nematic director must be considered. For a thermotropic mesogen with magnetic susceptibility anisotropy greater than zero ($\Delta\chi > 0$), which is the case of our compound, the helix axis arranges perpendicular to the magnetic field. Consequently, the line shape first originates from a distribution of different molecular orientations with respect to the magnetic field. Moreover, it can be deeply influenced by the diffusion of the molecules along the helix axis, depending on the ratio between the quadrupolar splitting and the exchange rate among sites with different orientations.[17] In the case of 11EB1M7-d_2, the experimental spectrum of the cholesteric mesophase at 107.5 °C (Figure 4) suggests that the sample experiences an intermediate exchange rate regime.[17]

The line shape characterizing the TGBA* mesophase (Figure 4) is very similar to that of the cholesteric one. The main difference is found comparing the overall line widths, which are, for instance, about 12 kHz for the TGBA* phase at 105.5 °C and about 5 kHz for the cholesteric phase at 107.5 °C. In fact, the TGBA* structure consists of a helicoidal distribution

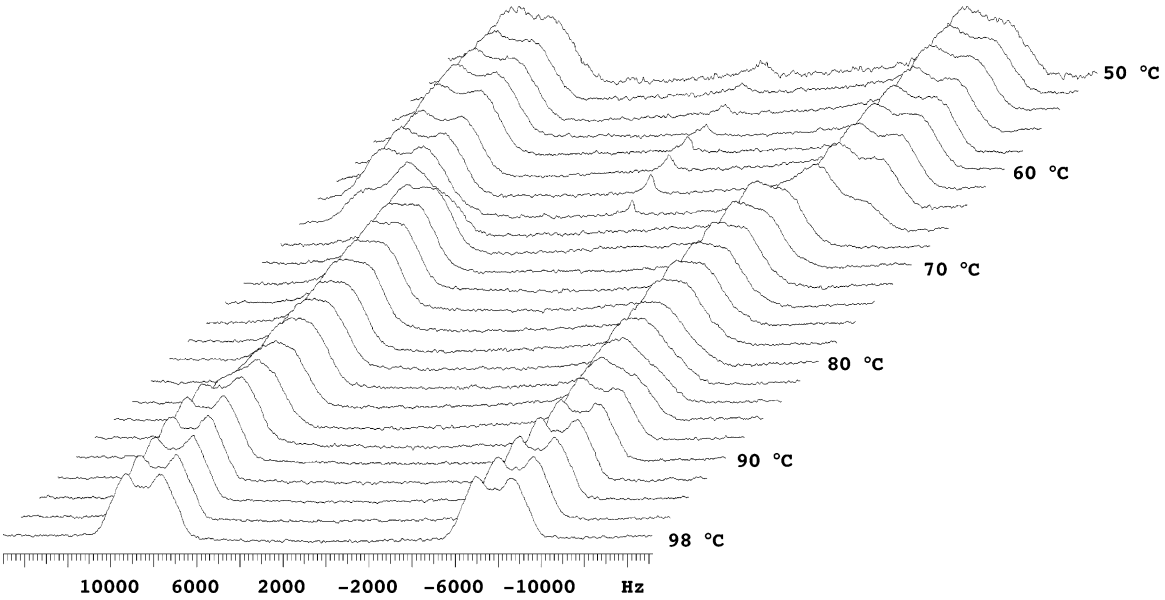

Figure 5. ^{2}H spectra of 11EB1M7-d_2 recorded at different temperatures in the SmA, SmC*, and SmI* phases.

of SmA blocks with a high local orientational order. The observed difference between line widths can be explained by an increase of the local order parameter by a factor of about 1.5 (comparable with typical values of the order parameter usually observed in the SmA (0.7−0.9) and nematic (0.4−0.6) mesophases[23,24]) together with an appreciable slowing of the molecular diffusion at low temperature.

Line Shapes, Order Parameters, and Tilt Angles in SmA, SmC*, and SmI* Phases

Different from the spectra discussed in the previous paragraph, those recorded in the SmA, SmC*, and SmI* phases show that the smectic planes are macroscopically ordered perpendicularly to the magnetic field. Moreover, the molecular director in the SmC* and SmI* phases is tilted with respect to the field.

The line shape simulations presented in this section were performed using a modified version of the "Lequor" software.[25] Figure 5 shows the ^{2}H NMR spectra of 11EB1M7-d_2 recorded in the temperature range 50−98 °C, in which three smectic phases are present. We can always observe a quadrupolar doublet, the components of which, in the SmA and SmI* phases, are further shaped and split by ^{1}H−^{2}H dipolar couplings. The most important dipolar interaction is between each deuterium nucleus and the nearest aromatic proton. Such interaction produces a doubling of the signals in the SmA and SmI* phases and just a broadening in the SmC* phase. The dipolar coupling between the deuterons and the protons of the nearest methylenic group in the alkoxylic chain also contributes to the signal shape. The simulation of the ^{1}H-coupled experimental spectrum at 98 °C (see Figure 6) in the SmA phase was performed by using the quadrupolar splitting and the line width determined from the ^{1}H-decoupled spectrum of 11EB1M7-d_2 and the $^1H_{aromatic}-^2$H dipolar coupling estimated from the splitting of each peak in the ^{1}H-coupled spectrum. A value for the $^1H_{methylenic}-^2$H dipolar coupling was taken from the corresponding ^{1}H−^{1}H dipolar coupling found for a similar compound in a nematic phase,[26] suitably scaled taking into account the different nuclei involved in the interaction and the different degree of orientational order. A satisfactory agreement between the experimental and simulated line shapes could be obtained by slightly adjusting the $^1H_{methylenic}-^2$H dipolar coupling and keeping all of the other parameters fixed at their original values. Good simulations of

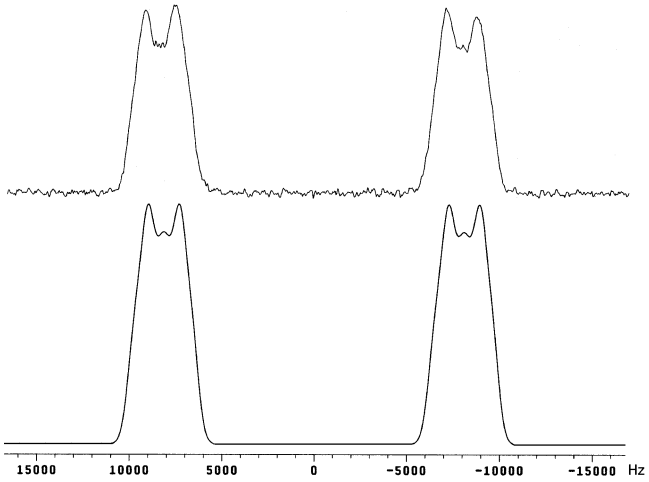

Figure 6. ^{2}H experimental (top) and simulated (bottom) spectra of 11EB1M7-d_2 at 98 °C in the SmA phase without proton decoupling.

the spectra at other temperatures in the smectic A and I* phases were also obtained, confirming that the $^1H_{aromatic}-^2$H dipolar splitting, $\Delta\nu_d$, which will appear in eq 3, could be directly determined from the splitting between the two maxima of each quadrupolar peak. In the SmC* phase, where the average observed interactions are substantially reduced by the tilt between the local directors and the magnetic field and this splitting is no longer resolved, the $^1H_{aromatic}-^2$H dipolar coupling could be estimated by the simulation procedure.

As far as 11EB1M7-d_8 is concerned (see, for example, the case T = 98 °C, reported in Figure 7), the ^{1}H-decoupled spectrum could be easily explained. Four quadrupolar doublets are expected because of the deuterons in the A, A′, B, and B′ positions (see Figure 1). The most intense signals are ascribed to the more abundant ortho deuterons A and A′, while two much weaker doublets, due to meta deuterons B and B′, are partially superimposed on them. To explain the ^{1}H-coupled spectrum, we must consider that the compound 11EB1M7-d_8 is, in effect, a mixture of 11EB1M7 molecules variously deuterated on the biphenyl fragment. The most abundant species is that deuterated only on the ortho positions. It contributes to the ^{1}H-coupled spectrum with the two intense quadrupolar doublets, the signals of which are split by the dipolar interaction between the deuteron

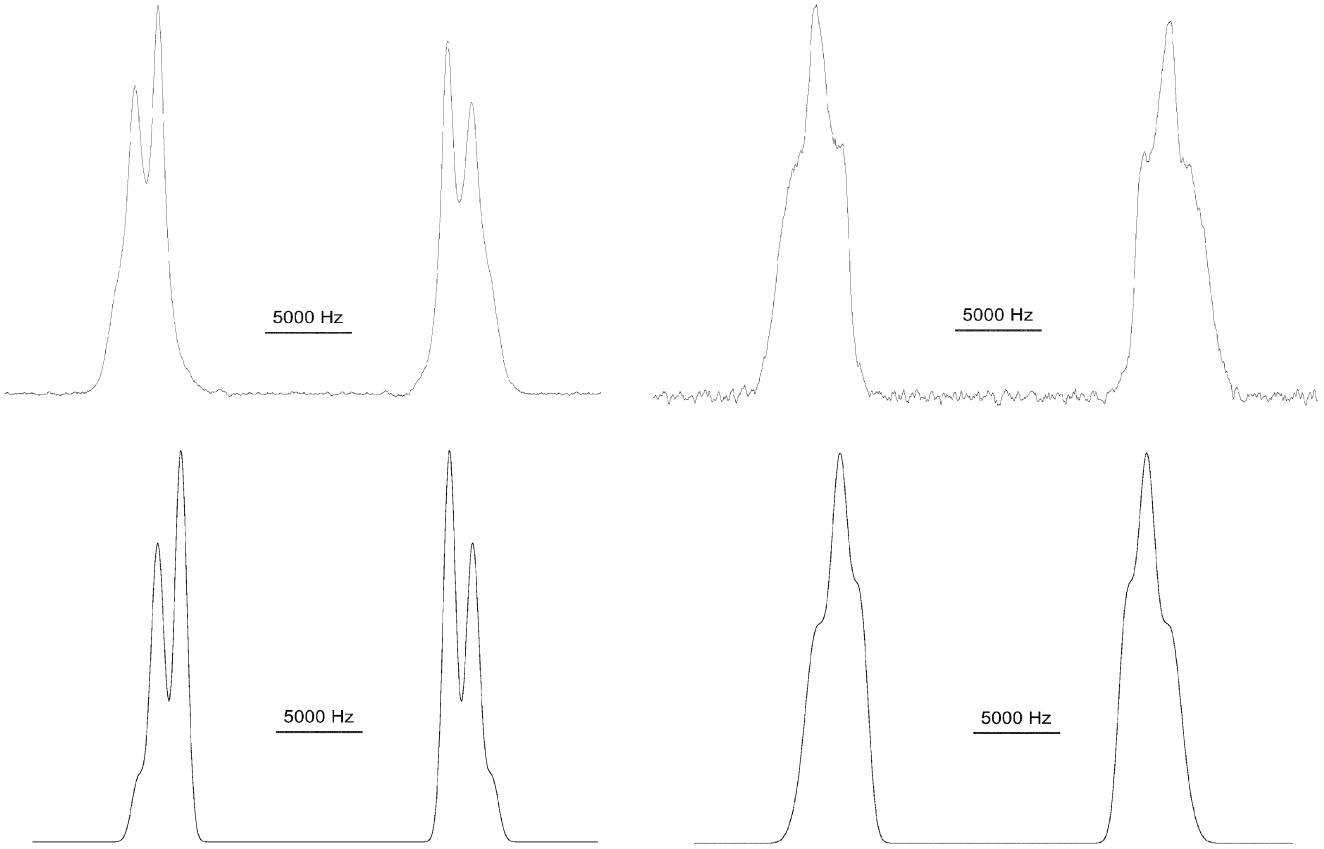

Figure 7. ^{2}H experimental (top) and simulated (bottom) spectra of 11EB1M7-d_8 at 98 °C in the SmA phase with proton decoupling (left) and without proton decoupling (right).

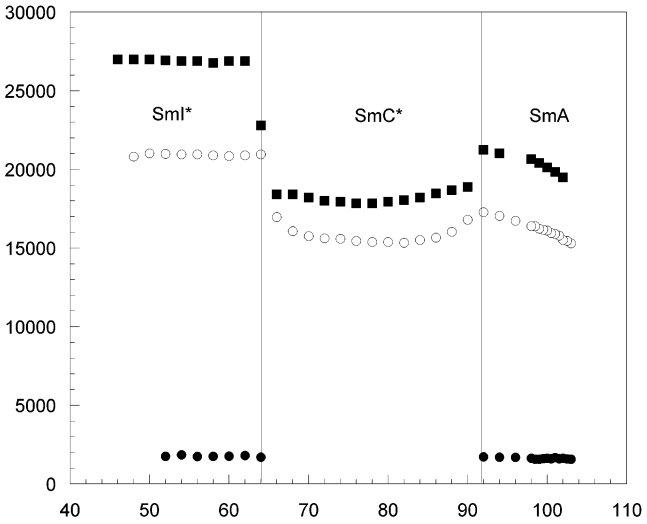

Figure 8. Quadrupolar (○ and ■ for d_2 and d_8 isotopomers, respectively) and ^{1}H−^{2}H dipolar (● for d_2 isotopomer) splittings (Hz) vs temperature (°C) measured for 11EB1M7 in the various smectic phases.

and the nearest proton. Therefore, the experimental line shape, roughly resembling an unresolved triplet, must be mostly ascribed to the partial superimposition of two dipolar doublets. An excellent agreement between the experimental and simulated line shape was then reached taking into account the composition of the mixture and building up a weighted superimposition of the spectra of the differently deuterated species. Relevant dipolar couplings are those between ortho−meta protons and deuterons and between the A′ deuteron and the near methinic proton. From simulations of spectra at various temperatures, we observed that the mean value of the two quadrupolar splittings of the ortho deuteria corresponds to the difference between the two maxima of the experimental quadrupolar doublet of the ^{1}H-coupled spectra.

The quadrupolar splitting of 11EB1M7-d_2 and the mean value of the two quadrupolar splittings of the ortho deuteria of 11EB1M7-d_8 are shown in Figure 8 as a function of temperature. In the SmA phase, the splittings regularly increase with decreasing temperature for both mesogens. Below the SmA−SmC* transition, a gradual decrease of the quadrupolar splittings takes place indicating a progressive tilt of the local directors with respect to the magnetic field. A jump to higher values is observed on entering the SmI* phase, followed by an almost constant trend within this phase. The $^1H_{aromatic}-^2H$ dipolar splitting trend vs temperature for the isotopomer 11EB1M7-d_2 is also reported in Figure 8. This splitting increases up to about 1700 Hz in the SmA phase, while in the SmC* one, it decreases to a minimum of 1440 Hz and then increases again up to about 1750 Hz, remaining constant within the experimental error limits in the SmI* phase.

We could eventually determine the order parameter $S_{ZZ}(T)$ and the biaxiality ($\Delta_{biax} = S_{XX} - S_{YY}$, assumed to be independent of temperature within each phase) for the two deuterated molecular fragments by fitting the experimental values of the $^1H_{aromatic}-^2H$ dipolar and quadrupolar splittings by eqs 3 and 4[2]:

$$\Delta\nu_d[T] = -2K_{DH}\frac{S_{zz}[T]}{r_{DH}^3} \qquad (3)$$

$$\Delta\nu_q[T] = \frac{3}{2}q_{aa}\left\{S_{zz}[T]\left(\cos^2\phi - \frac{1}{2}\sin^2\phi - \frac{\eta}{6}\cos^2\phi + \frac{\eta}{6} + \frac{\eta}{3}\sin^2\phi\right) + \Delta_{biax}\left(\frac{1}{2}\sin^2\phi + \frac{\eta}{6}\cos^2\phi + \frac{\eta}{6}\right)\right\} \quad (4)$$

where $K_{DH} = 18\,434.4$ Hz·Å^3, $r_{DH} = 2.5$ Å, $\eta = 0.04$, and $q_{aa} = 185$ kHz. The angle ϕ between the C−D bond and the para axis of the rigid fragment has been assumed equal to 60° in all cases. For the phenyl fragment of 11EB1M7-d_2, the best-fitting parameters for Δ_{biax} are 0.047, 0.039, and 0.019 in the SmA, SmC*, and SmI* phases, respectively, while those for S_{ZZ} at the different temperatures are reported in Figure 9.

For the isotopomer 11EB1M7-d_8, the dipolar splittings could not be directly measured from the spectra; their values, determined by the line shape simulation, allowed us to verify that the biaxiality is about zero, in agreement with the results obtained for a very similar compound.[6] The trend of the order parameter S_{ZZ} of the biphenyl fragment, which could be therefore calculated from the quadrupolar splittings measured for 11EB1M7-d_8 by eq 4, is also reported in Figure 9.

In both smectogens, the SmA−SmC* transition is evident from the sudden decrease of the order parameters. The tilt angle θ in the tilted SmC* phase could be estimated by assuming that the deviation from a regular order parameter trend is fully ascribable to the tilt of the molecules with respect to the magnetic field. To this aim, the order parameter trend in the untilted SmA phase has been extrapolated in the tilted smectic phase for the two isotopomers, and the tilt angles have been determined by the ratios of the so-calculated and experimental S_{ZZ} values as described by eq 5:

$$S_{ZZ}^{exptl} = S_{ZZ}^{calcd}\frac{3\cos^2\theta - 1}{2} \quad (5)$$

The tilt angles obtained independently for the two sets of data (phenyl and biphenyl order parameters) show a good agreement, and their average value increases by decreasing the temperature within the SmC* phase assuming a limiting value of 18°.

At the SmC*−SmI* transition, a dramatic change in the order parameter trends can be observed: on one side, the S_{ZZ} of both fragments experiences a jump to higher values; on the other side, within the SmI* phase, the S_{ZZ} of the biphenyl fragment is higher than that of the phenyl fragment, contrary to what is observed within the SmA and SmC* phases. The S_{ZZ} jump indicates a sudden decrease of the tilt angle on entering the SmI* phase. Moreover, the biphenyl fragment becomes so ordered in the SmI* phase ($S_{ZZ} \approx 0.9$) that its para axis can be substantially assumed to be aligned to the magnetic field.

On the other hand, when the para axis of one aromatic moiety is aligned to the magnetic field, the angle φ between the para axes of the phenyl and biphenyl fragments can be evaluated on the basis of eq 6.

$$S_{ZZ}^{I} = S_{ZZ}^{II}\frac{3\cos^2\varphi - 1}{2} \quad (6)$$

where I and II correspond to the less- and more-ordered fragments, respectively. The values of φ so calculated in the SmA and SmI* phases are substantially constant within each phase, and the average value of φ is 11.6° ± 1.5° in the SmA phase and 18.2° ± 0.5° in the SmI* phase, in good agreement with values previously obtained for a similar compound.[6]

Dynamics: Theory

The Redfield theory directly relates the quadrupolar (T_{1Q}) and Zeeman (T_{1Z}) spin−lattice relaxation times to the spectral densities of motion, $J_i(i\omega_0)$ (which are the Fourier transforms of the autocorrelation functions), at the Larmor frequency and at twice this frequency through the following relationships:

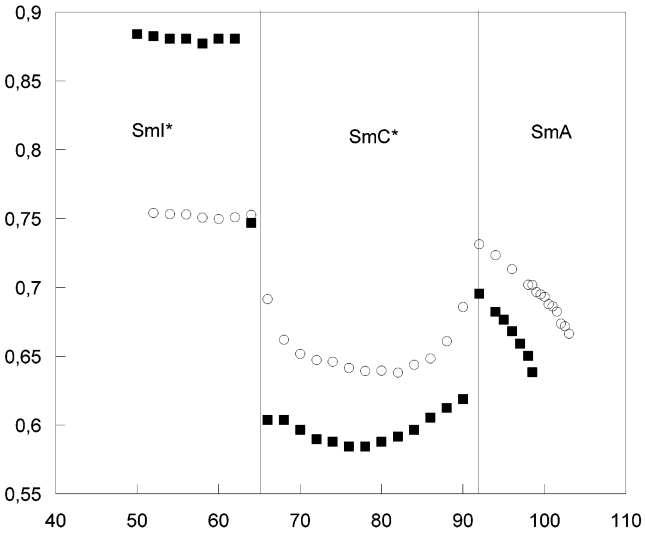

Figure 9. Order parameter S_{zz} of the phenyl (○) and biphenyl (■) fragments as a function of temperature (°C).

$$\frac{1}{T_{1Z}} = J_1(\omega_0) + 4J_2(2\omega_0) \quad (7)$$

$$\frac{1}{T_{1Q}} = 3J_1(\omega_0) \quad (8)$$

where ω_0 is the Larmor frequency. Several motional processes contribute to these spectral densities, which can be classified in three distinct types: overall reorientations of the whole molecule, internal motions of molecular fragments, and collective motions. However, the information on these motions is contained in a quite implicit form within the spectral densities, and therefore, its extraction requires the use of suitable theoretical models.

Several models have been proposed to describe the overall molecular reorientations, going from the simplest *diffusion in a cone*[27] to those proposed by Nordio et al.[28,29] and by Freed et al.[30,31] (*anisotropic viscosity* model), which consider these motions as small step diffusional rotation in a Maier−Saupe mean field potential, up to the extensions of Vold and Vold[32] (*third rate anisotropic viscosity* model), of Tarroni and Zannoni,[33] and of Berggren et al.,[34] the last two models taking into account either molecular or phase biaxiality.

Internal motions are usually considered decoupled from the overall molecular ones. In particular, aromatic ring rotations have been described in an isotropic potential by means of either small step diffusion[35,36] or strong collision models[37] or in a 2-fold symmetric intramolecular potential considering coupled rotational isomerization and libration processes.[38]

Collective motions essentially consist of order director fluctuations (ODF), which are usually considered not coupled to the faster overall and internal molecular motions; their contribution to the spectral densities can be expressed on the basis of the theories proposed by Pincus[39] and Blinc et al.[40] Other slower collective dynamic processes can be present in tilted smectic phases, such as the Goldstone and soft modes,[1] but their contribution to the spectral densities in the megahertz range is usually negligible.

The analysis of the relaxation data has been here carried out using the Nordio model for the overall dynamics, using both

small step diffusion and strong collision for the internal rotation of either phenyl or biphenyl fragments about their para axes, and neglecting the contribution of ODF. This assumption is based on the theoretical prediction of a null contribution to $J_2(2\omega_0)$ and of a contribution to $J_1(\omega_0)$ that is directly proportional to $\omega_0^{-1/2}$ and to the geometrical term $(3\cos^2\beta - 1)$, β being the angle between the C−D bond and the axis of the fragment under examination. Indeed, in our case, the Larmor frequency and β are, respectively, high enough (46.04 MHz) and close enough to the magic angle (60°) to safely allow the ODF contribution to be neglected.

The autocorrelation functions, $g_{m_L m_M}(t)$, relative to the overall molecular motions, can be expressed, following Vold and Vold,[32] as a sum of decreasing exponential functions:

$$g_{m_L m_M}(t) = c_{m_L m_M} \sum_j a^{(j)}_{m_L m_M} \exp\left(-\frac{t}{\tau^{(j)}_{m_L m_M}}\right) \qquad (9)$$

The correlation times, $\tau^{(j)}_{m_L m_M}$, can be expressed in terms of the diffusional coefficients on the basis of Nordio model through the following relationship:

$$\frac{1}{\tau^{(j)}_{m_L m_M}} = \frac{6D_\perp}{b^{(j)}_{m_L m_M}} + m_M{}^2(D_\parallel - D_\perp) \qquad (10)$$

where $D_\parallel$ and $D_\perp$ are the principal components of the diffusion tensor, diagonalized in a molecular frame, describing the molecular spinning and tumbling motions, respectively, and the coefficients $a^{(j)}_{m_L m_M}$, $b^{(j)}_{m_L m_M}$, and $c_{m_L m_M}$ have been calculated in ref 32 as a function of the principal order parameter for a Maier−Saupe potential.

The internal motions can be "superimposed" to the overall molecular motions by taking the products of the respective autocorrelation functions, which can be Fourier-transformed to give eventually the following expression for J[3]:

$$J_{m_L}(m_L\omega_0) = \frac{3\pi^2}{2}(\nu_q)^2 \sum_{m_M=-}^{2} \sum_{2m_R=-2}^{2} c_{m_L m_M}[d_{m_R 0}{}^2(\beta_{i,Q_i})]^2[d_{m_M m_R}{}^2(\beta_{M,i})]^2 \sum_j a^{(j)}_{m_L m_M} \frac{(\tau^{(j)}_{m_L m_M})^{-1} + \xi(m_R)D_i}{(m_L\omega_0)^2 + [(\tau^{(j)}_{m_L m_M})^{-1} + \xi(m_R)D_i]^2} \qquad (11)$$

where ν_q is the quadrupolar coupling constant, $d_{rs}{}^2$ are the reduced Wigner matrices, β_{i,Q_i} is the angle between the C−D bond and the axis about which the internal rotation takes place, $\beta_{M,i}$ is the angle between this axis and the molecular long axis, D_i is the diffusion coefficient relative to the internal rotation of the fragment considered, and $\xi(m_R)$ is $(1 - \delta_{m_R})$ or $m_R{}^2$ if the strong collision or small step diffusion models are used, respectively, for this motion.

Dynamics: Results and Discussion

The deuterium relaxation times T_{1Z} and T_{1Q} have been measured in the two isotopomers by means of the broadband Jeener−Broekaert pulse sequence throughout the mesophasic range. A single relaxation time has been determined in the case of the isotopomer d_8 for all of the deuterium nuclei, because of the difficulty of extracting individual contributions of different biphenyl deuteria to the whole spectrum; a close inspection of the relaxation trend, however, did not allow any difference to be revealed among the different components of the line shape.

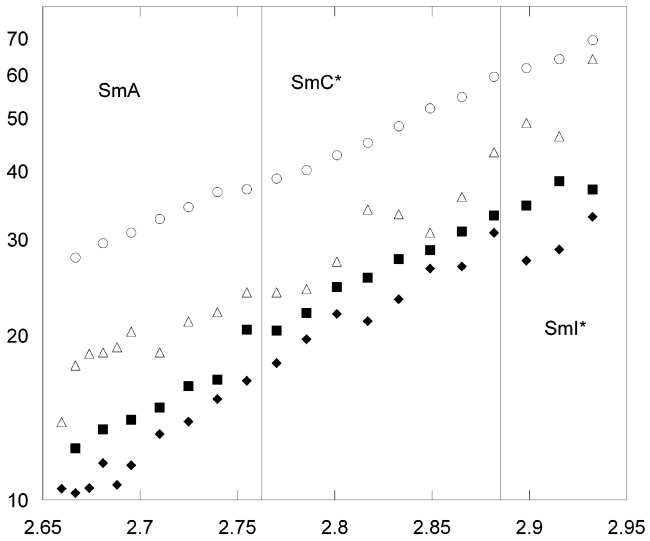

Figure 10. Experimental spectral densities (s^{-1}), $J_1(\omega_0)$ (○ and △ for d_2 and d_8 isotopomers, respectively) and $J_2(2\omega_0)$ (■ and ◆ for d_2 and d_8 isotopomers, respectively), of 11EB1M7 in the SmA, SmC*, and SmI* phases vs $1000/T$ (1/K).

From the measured relaxation times, which are on the order of tens of milliseconds, the corresponding spectral densities have been calculated by eqs 7 and 8 (see Figure 10). The spectral densities decrease with increasing temperature, indicating a motional narrowing regime ($\omega_0\tau_c \ll 1$) for the motions mainly contributing to the relaxation, in agreement with what is usually found for low-molecular-weight liquid crystals.[9,41,42] The trends of the various relaxation times and corresponding spectral densities do not show any particular discontinuity throughout the temperature range investigated, as already observed for both ^{2}H[9] and ^{13}C[43] spin−lattice relaxation times of other ferroelectric liquid crystals. This is a clear indication of the absence of dramatic changes in the motional processes occurring in the megahertz range over the different mesophases and, in particular, at the transition between untilted (smectic A) and tilted (smectic C*) phases.

A more detailed, quantitative analysis of the spectral densities could be performed on the basis of existing diffusional models only in the untilted smectic A phase because of the lack of specific models for tilted smectic phases. However, a procedure that allows the analysis of the spectral densities in terms of diffusional coefficients to be extended to tilted phases has been recently developed in our group,[44] and the data analysis for 11EBM7 and other ferroelectric liquid crystals is currently in progress.

The relaxation data in the smectic A phase were analyzed using a global target approach by assuming an Arrhenius behavior for the four diffusional coefficients ($D_\parallel$ and $D_\perp$ for molecular spinning and tumbling, and $D_{R(phe)}$ and $D_{R(biphe)}$ for the rotation of the phenyl and biphenyl fragments about their para axes). Moreover, the ratio $D_\parallel/D_\perp$ was fixed to the value of 11, arising from the application of the model proposed by Perrin,[45] which gives an estimate of this value on the basis of the ratio between the semiaxes of the ellipsoid to which the molecule is approximated. In fact, it has been recently shown[9,42] that when relaxation data at a single Larmor frequency or of only few different deuterons or both are available, the diffusional coefficient for the tumbling motion exhibits a high indeterminacy and constraints must be applied to obtain physically meaningful results. The values of the order parameter relative

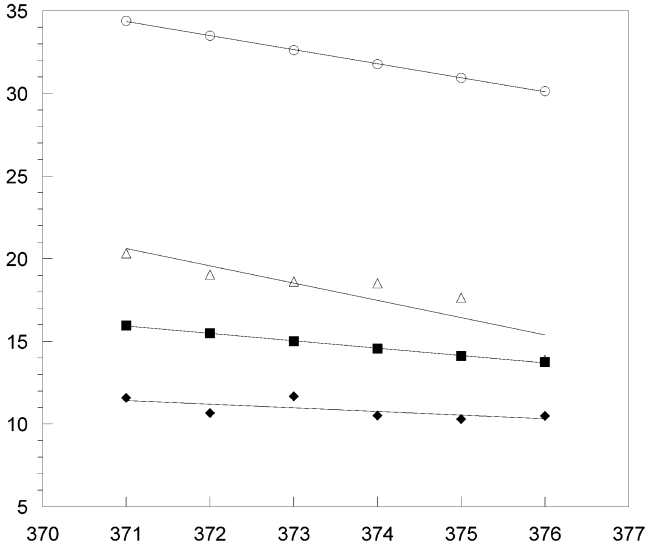

Figure 11. Calculated (lines) and experimental (symbols) spectral densities (s^{-1}), $J_1(\omega_0)$ (○ and △ for d_2 and d_8 isotopomers, respectively) and $J_2(2\omega_0)$ (■ and ◆ for d_2 and d_8 isotopomers, respectively), of 11EB1M7 in the SmA phase vs T (K).

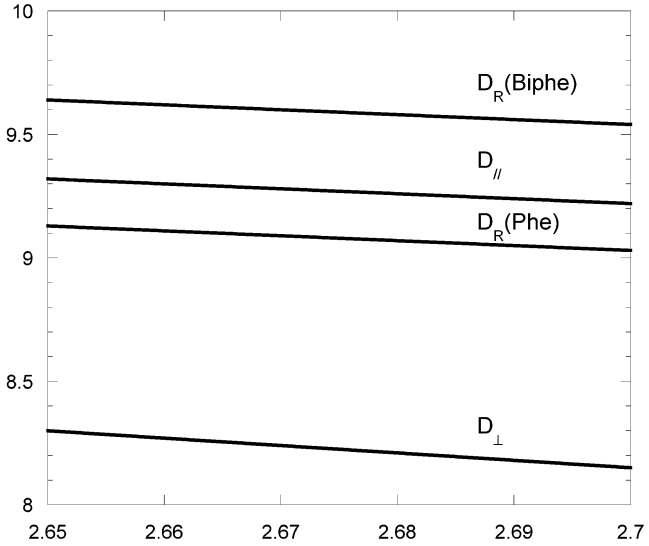

Figure 12. Logarithm of the diffusional constants $D_{||}$, $D_{\perp}$, $D_{R(phe)}$, and $D_{R(biphe)}$ (s^{-1}) vs 1000/T (1/K) derived by a global target procedure using superimposed Nordio and strong collision models (see text).

to the phenyl moiety (the para axis of which is assumed to be aligned to the magnetic field) reported in the Line Shapes, Order Parameters, and Tilt Angles in SmA, SmC*, and SmI* Phases section were used. In agreement with the orientational order data analysis, the angle β_{i,Q_i} was taken as 60° for all of the deuterons, the molecular long axis was assumed to be parallel to the para axis of the phenyl fragment, and the angle between the molecular long axis and the para axis of the biphenyl fragment was taken from the results obtained by the ratio of the order parameters of the two aromatic fragments. The analysis performed using the strong collision model for the internal motions gave a very good agreement between calculated and experimental spectral densities for all of the deuterons over the whole SmA range, as shown in Figure 11.

The diffusional coefficients obtained for the spinning and tumbling molecular motions, as well as for the internal motions of both the phenyl and the biphenyl moieties, are reported in Figure 12. It can be noticed that diffusional coefficients for the two internal motions are of the same order of magnitude of the diffusional coefficients for the spinning motion, which is intermediate between them, being slightly higher than those of the reorientational motion of the phenyl ring.

The values of both diffusional constant and activation energies (40 kJ/mol for $D_{||}$ and $D_{\perp}$, and 32 kJ/mol for $D_{R(phe)}$ and $D_{R(biphe)}$) are in general agreement with those previously found for similar smectogens.[9,41,46] The errors of the Arrhenius preexponential coefficients are 5% for $D_{||}$ and 10% for $D_{R(phe)}$ and $D_{R(biphe)}$, while those of the activation energies are 0.5% and 1% for the spinning and internal motions, respectively.

A satisfactory reproduction of the experimental data could not be obtained by using the small step rotational diffusion model in place of the strong collision one for the internal reorientation of either the phenyl or the biphenyl group. This is a quite unusual behavior, because usually the two models are equally suitable to describe the internal dynamics of aromatic fragments in achiral low-molecular-weight liquid crystal. However, the same discrimination between the two models was previously observed by us in the SmA phase of the ferroelectric liquid crystal 8BEF5.[10] The results here shown thus further support the hypothesis that internal motions of aromatic fragments may have a peculiar behavior in the SmA phases of FLCs.

Conclusions

^{2}H NMR was employed to investigate the orientational order and the dynamic properties of the liquid crystalline phases of the smectogen 11EB1M7 by using two different selectively ^{2}H-labeled isotopomers. The line shape behavior of the ^{2}H NMR spectra has been used to follow the phase transitions. From the quadrupolar and dipolar splittings, the orientational order parameters of the rigid phenyl and biphenyl fragments were obtained as a function of the temperature. The tilt angle within the SmC* phase, as well as the angle between the para axes of the phenyl and biphenyl aromatic fragments within the SmA and SmI* phases, could be estimated from the S_{ZZ} ratios. The change in the relative orientation of the two aromatic fragments with respect to the magnetic field occurring at the SmC*−SmI* transition, allowed by the noncollinearity of their para axes, is in agreement with the more solidlike structure of the SmI* phase, where the more bulky biphenyl fragment becomes the more ordered one, perhaps because of more constrained packing interactions. This behavior is possibly related to the different angle between the para axes of the two fragments estimated in the SmI* phase with respect to the SmA one.

The dynamic behavior of 11EB1M7 was investigated in its smectic A and C* phases. The spectral density data of the phenyl and biphenyl deuterons could be quantitatively analyzed in terms of diffusional models only in the smectic A phase by superimposing internal rotations of each fragment onto the overall molecular reorientations. The diffusional coefficients of the internal rotations of both the phenyl and biphenyl rings have been found to be of the same order of magnitude of those of the molecular spinning and approximately 1 order of magnitude higher than those of the molecular tumbling. Contrary to what has been observed for achiral low-molecular-weight liquid crystals, only the strong collision model could suitably describe the internal motions of the aromatic fragments around their para axes, confirming previous results and suggesting a peculiar dynamic behavior of FLCs.

Acknowledgment. We thank the Italian MIUR for partial financial support. Special thanks to Prof. G. Galli and Prof. K. Fodor-Csorba for their collaboration.

References and Notes

(1) Musevic, I.; Blinc, R.; Zeks, B. *The Physics of ferroelectric and antiferroelectric liquid crystals*; World Scientific: Singapore, 2000.

(2) Veracini, C. A. NMR Spectra in Liquid Crystals the Partially Averaged Spin Hamiltonian. In *Nuclear Magnetic Resonance of Liquid Crystals*; Emsley, J. W., Ed.; Reidel: Dordrecht, Netherlands, 1985; Vol. 141, Chapter 5, p 99.

(3) Dong, R. Y. In *Nuclear Magnetic Resonance of Liquid Crystals*; Springer- Verlag: New York, 1997.

(4) Dong, R. Y. *Prog. Nucl. Magn. Reson.* **2002**, *41*, 115.

(5) Geppi, M.; Veracini, C. A. Chiral smectic phases: NMR studies. In *Encyclopedia of Nuclear Magnetic Resonance*; Grant, D. M., Harris, R. K., Eds.; John Wiley and Sons: Chichester, U.K., 2002; Vol. 9, pp 506−513.

(6) Catalano, D.; Cavazza, M.; Chiezzi, L.; Geppi, M.; Veracini, C. A. *Liq. Cryst.* **2000**, *27*, 621.

(7) Catalano, D.; Chiezzi, L.; Domenici, V.; Geppi, M.; Veracini C. A.; Dong, R. Y.; Fodor-Csorba, K. *Macromol. Chem. Phys.* **2002**, *203*, 1594.

(8) Catalano, D.; Cifelli, M.; Fodor-Csorba, K.; Gacs-Baitz, E.; Geppi, M.; Jakli, A.; Veracini, C. A. *Mol. Cryst. Liq. Cryst.* **2000**, *351*, 245.

(9) Catalano, D.; Cifelli, M.; Geppi, M.; Veracini, C. A. *J. Phys. Chem. A* **2001**, *105*, 34.

(10) Chiezzi, L.; Domenici, V.; Geppi, M.; Veracini, C. A.; Dong, R. Y. *Chem. Phys. Lett.* **2002**, *358*, 257.

(11) Catalano, D.; Chiezzi, L.; Domenici, D.; Galli, G.; Veracini, C. A. *Mol. Cryst. Liq. Cryst.* **2003**, *398*, 127.

(12) Ragnoli, M. Master Thesis, Università di Pisa, Pisa, Italy, 1999.

(13) Wimperis, S. *J. Magn. Reson.* **1990**, *86*, 46.

(14) Jeener, J.; Broekaert, P. *Phys. Rev.* **1967**, *157*, 232.

(15) Catalano, D.; Ciampi, E.; Fodor-Csorba, K.; Forte, C.; Geppi, M.; Imbardelli, D. *Liq. Cryst.* **1996**, *21*, 927.

(16) Vold, R.; Vold, R. In *The Molecular Dynamics of Liquid Crystals*; Luckurst, G. R., Veracini, C. A., Eds.; Kluwer: Dordrecht, Netherlands, 1994.

(17) Luz, Z.; Poupko, R.; Samulski, E. T. *J. Chem. Phys.* **1981**, *74*, 5825.

(18) Samulski, E. T.; Luz, Z. *J. Chem. Phys.* **1980**, *73*, 142.

(19) Yaniv, Z.; Chidichimo, G.; Doane, J. W. *Phys. Rev. A* **1983**, *28*, 3012.

(20) Vaz, N.; Chidichimo, G.; Yaniv, Z.; Doane, J. W. *Phys. Rev. A* **1982**, *26*, 637.

(21) Vaz, N.; Chidichimo, G.; Yaniv, Z.; Doane, J. W. *Phys. Rev. A* **1982**, *25*, 1077.

(22) Shivaprakash, N.; Shashidhara-Prasad, J. *J. Chem. Phys.* **1982**, *76*, 1209.

(23) McMillan, W. L. *Phys. Rev. A* **1971**, *4*, 1238.

(24) McMillan, W. L. *Phys. Rev. A* **1972**, *6*, 936.

(25) Dichl, P.; Kellerhals, H. P.; Niederberger, W. *J. Magn. Reson.* **1971**, *4*, 352.

(26) Emsley, J. W.; Celebre, G.; De Luca, G.; Longeri, M.; Catalano, D.; Veracini, C. A. *Gazz. Chim. Ital.* **1996**, *126*, 429.

(27) Wang, C. C.; Pecora, R. *J. Chem. Phys.* **1980**, *72*, 5333.

(28) Nordio, P. L.; Busolin, P. *J. Chem. Phys.* **1971**, *55*, 5485.

(29) Nordio, P. L.; Rigatti, G.; Segre, U. *J. Chem. Phys.* **1972**, *56*, 2117.

(30) Polnaszek, C. F.; Bruno, G. V.; Freed, J. H. *J. Chem. Phys.* **1975**, *58*, 3185.

(31) Polnaszek, C. F.; Freed, J. H. *J. Phys. Chem.* **1975**, *79*, 2283.

(32) Vold, R. R.; Vold, R. L. *J. Chem. Phys.* **1988**, *88*, 1443.

(33) Tarroni, R.; Zannoni, C. *J. Chem. Phys.* **1991**, *95*, 4550.

(34) Berggren, E.; Tarroni, R.; Zannoni, C. *J. Chem. Phys.* **1993**, *99*, 6180.

(35) Woessner, D. E. *J. Chem. Phys.* **1962**, *36*, 1−4.

(36) Dong, R. Y. *Mol. Cryst. Liq. Cryst.* **1986**, *141*, 349.

(37) Beckmann, P. A.; Emsley, J. W.; Luckurst, G. R.; Turner, D. L. *Mol. Phys.* **1986**, *59*, 97.

(38) Heaton, N. J.; Kothe, G. *J. Chem. Phys.* **1998**, *108*, 8199.

(39) Pincus, P. *Solid State Commun.* **1969**, *7*, 415.

(40) Blinc, R.; Hogenboom, D.; O'Reilly, D.; Peterson, E. *Phys. Rev. Lett.* **1969**, *23*, 969.

(41) Calucci, L.; Catalano, D.; Fodor-Csorba, K.; Forte, C.; Veracini, C. A. *Mol. Cryst. Liq. Cryst.* **1999**, *9*, 331.

(42) Calucci, L.; Geppi, M. *J. Chem. Inf. Comput. Sci.* **2001**, *41*, 1006.

(43) Yoshizawa, A.; Yokoyama, A.; Kikuzaki, H.; Hirai, T. *Liq. Cryst.* **1993**, *14*, 513.

(44) Domenici, V.; Geppi, M.; Veracini, C. A. *Chem. Phys. Lett.*, submitted for publication, 2003.

(45) Perrin, F. *J. Phys. Radium* **1934**, *5*, 497.

(46) Calucci, L.; Geppi, M.; Veracini, C. A.; Dong, R. Y. *Chem. Phys. Lett.* **1998**, *296*, 357.